Transactions of the Korean Nuclear Society Fall Meeting
Jeju, Korea, May. 16-18, 2018

Role of Aluminum Oxide Thin Film on Crud Deposition of the Fuel Cladding in a Primary Water of PWRs

Hee-Sang Shim*, Moon-Sic Park, Seung Heon Baek, Do Haeng Hur

Nuclear Materials Research Division, KAERI, 989-111 Daedeok-daero, Yuseong-gu, Daejeon 34057, Korea
**Corresponding author: hshim@kaeri.re.kr*

1. Introduction

As pressurized water reactors (PWRs) have been recently driven to power uprate, lifetime extension and higher burnup for enhancing economics of power generation, some reactors have experienced an increase of deposits on the fuel assemblies [1,2]. These deposits are called as 'crud' and arise from corrosion products released from the surfaces of the reactor coolant system (RCS). It is well known that crud has a porous structure because crud deposition is stimulated in a condition where sub-cooled nucleate boiling (SNB) occurs [3].

Various chemical species included in a primary coolant can be accumulated in the porous crud. Among them, concentrated boron-containing compounds can induce local power shift owing to neutron capture by boron, resulting in power output de-rating [4,5]. Lithium can also be concentrated inside the pores, elevate pH there, and increases the corrosion rate of fuel claddings. In addition, the crud on fuel assemblies can increase fuel cladding temperature due to increased thermal resistance, resulting in accelerated fuel cladding corrosion [6,7]. A part of crud activated on fuel assemblies is released again into the primary coolant, transported out of core, and deposited on ex-core surfaces, resulting in increased occupational radiation exposure.

Thus, several methods have been implemented to plants to mitigate the above-mentioned problems caused by crud. Elevated pH_T operation of the reactor coolant chemistry from 6.9 to 7.2-7.4 shows a reduction in crud deposition in PWRs [8,9]. Ultrasonic fuel cleaning technology has been also used to remove crud from the reloaded fuel assemblies during outage [10]. In addition, various mitigation methods such as passivation of steam generator (SG) tubes, electropolishing SG channel head, and reducing roughness of SG tubes have also been suggested for reducing radiation source terms in PWRs [11-13].

After the accident at Fukushima Daiichi in 2011, development of accident tolerance fuel (ATF) claddings have become an important research topic worldwide. One of the ATF options is to use a coated zirconium alloy cladding that can provide the necessary protection during an off-normal high temperature or loss of coolant accident (LOCA) conditions. The coating materials and their deposition technologies considered were extensively reviewed in the literature [14]. Similarly, Dumnernchanvanit et al. have recently reported on the initial experimental results of crud-resistant materials as fuel cladding coatings to reduce crud deposition [15].

In this work, we coated aluminum oxide (Al_2O_3) thin layer on a ZILRO™ fuel cladding tube by using the atomic layer deposition (ALD) technique. Crud deposition tests were performed to quantify the relative crud mass under a sub-cooled nucleate flow boiling condition in a simulated primary water at 328°C. The obtained results are discussed in the view point of electrostatic forces between magnetite particle and cladding surfaces, and wettability of the cladding surfaces.

2. Experimental

Al_2O_3 was chosen as a coating material, based on its thermal compatibility with Zr-based cladding alloys in neutron cross section and thermal property. A commercial ZIRLO™ cladding tube was used as the substrate for the coating. The cladding tube has a dimension of a 9.5 mm outer diameter (OD) and an 8.3 mm inner diameter. This tube was cut into tubular segments with a length of 6 mm and then the rings were ultrasonically cleaned in acetone and ethanol for 5 min. A part of the cladding tube was also segmented in small rectangle pieces and their OD sides were ground with SiC papers to have a flat surface for measurement of the wettability and surface zeta potential. At this time, the roughness of the flat surface was controlled to be the same as that of the as-received cladding tube.

Al_2O_3 layer was deposited using ALD technique on the surface of the tubular and flat segments. ALD of Al_2O_3 layer was conducted at 250°C with trimethyl-aluminum ($Al(CH_3)_3$, TMA) and de-ionized water (DIW) as reactants. One cycle of thermal ALD Al_2O_3 growth consisted of a pulse of TMA, followed by a pulse of DIW. Each step was carried by a flow of nitrogen gas and separated by purge time. Two processes were performed alternately 200 times.

The ring specimens of as-received (or uncoated) and Al_2O_3-coated segments were put on a cartridge heater. The diameter of the heater was designed to provide tight thermal contact with the ring specimens. Test solution was prepared by dissolving chemicals of LiOH and H_3BO_3 into high purity DIW. The prepared solution chemistry was 3.5 ppm Li and 1500 ppm B in weight, which was used to simulate a primary water in PWRs. This solution of 200 liters was stored in the solution tank.

The sources of Ni and Fe ions for crud deposition were prepared using Ni- and Fe-ethylenediamine tetraacetic acid (EDTA), respectively. The mixed source solution of 1000 ppm Fe + 40 ppm Ni in weight was stored in the injection tank for injection to the test section.

Crud deposition tests were performed in a 316 stainless steel autoclave connected to a primary water recirculating loop as schematically shown in Fig. 1. The pressure of the test section was regulated at 130 bars.

Dissolved oxygen was maintained to be less than 5 ppb and dissolved hydrogen was controlled to be 35 $cm^3/kg \cdot H_2O$ (STP) by controlling the hydrogen overpressure of the solution tank. The flow rate at the surface of fuel cladding was controlled at 5 m/sec.

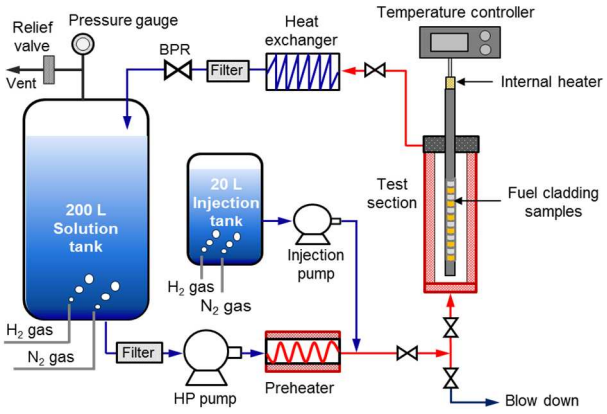

Fig. 1 Schematic of the test loop for crud deposition.

The inlet solution was injected into the test section through preheating and the temperature of the flowing water adjacent to the ring specimens was maintained at 328°C. The temperature of the internal heater was maintained at 380°C to provide the SNB condition on the ring specimen surface during crud deposition tests. At this time, the active SNB condition has been already confirmed through our previous study [16,17].

The crud source solution containing the Fe and Ni ions was injected with a flow rate of 1.1 ml/min from the injection tank to the test section via the metering injection pump after all these conditions were stabilized. This precursor solution was diluted in the simulated primary water stream and then its final chemistry was calculated to be 4.0 ppm Fe and 0.16 ppm Ni in the test section. The deposition test was conducted for 168 h.

To characterize the wettability of the uncoated and Al_2O_3-coated specimen surfaces, the static contact angle was measured at 25°C. A DIW droplet of 3 $\mu\ell$ was placed by a syringe vertically down onto the specimen surface. The image of the droplet was then captured by a high resolution digital camera, and the static contact angle was finally determined by using image analysis software. Measurements were made at five different points on a specimen surface and the mean value was reported together with the standard deviation.

The zeta potential measurement was performed using a Malvern Zetasizer Nano ZS system equipped with a surface zeta potential cell kit. Magnetite nanoparticles with an average size of 5 nm were diluted in high purity DIW to be a concentration of 5 mg/l. The diluted solution was transferred to a measurement cell. The surface zeta potentials of the two different surfaces were also measured using the surface zeta potential cell kit. A flat sample was mounted between two electrodes and immersed in the solution containing tracer magnetite nanoparticles. This solution was the same as used for zeta potential measurement of magnetite nanoparticles. The apparent tracer mobility was measured at a number of different distances from the sample surface. Every measurement was conducted at 25°C and repeated at least 3 times.

The deposits on the surface of ring specimens were dissolved in aqua regia solution after deposition tests. Then, the insides of the specimens were plugged by resin to analyze only the outside surface. Then, the concentrations of Ni and Fe were analyzed using an inductively coupled plasma-atomic emission spectroscope (ICP-AES). To calculate the quantity of the crud, the mass of Ni and Fe, determined by ICP-AES, was divided by the outside surface area of the ring specimen. The morphology of the crud was analyzed using a scanning electron microscope (SEM). In addition, the crud structure formed on the specimens was analyzed using x-ray diffraction (XRD). The thickness of the coated Al_2O_3 layer was determined using focused ion beam (FIB) milling technique, and the chemical composition across the interface between crud and matrix was analyzed using an energy dispersive x-ray spectroscopy (EDS).

3. Results and discussion

Fig. 2 shows the TEM-EDS results on the cross-section of the Al_2O_3-coated specimen, which was processed using FIB. It was observed that the Al_2O_3 layer was very dense and uniformly deposited on the cladding surface. The average thickness of the Al_2O_3 layer was measured to be about 22 nm. Zirconium oxide (ZrO_2) layer about 20 nm thick was also observed beneath the coated layer, which may be formed during the ALD coating process. The atomic ratio of oxygen to aluminum in the coated layer was calculated to be near 1.5 from the EDS data. Furthermore, the TEM micrograph and FFT pattern revealed that the Al_2O_3-coated layer had an amorphous structure.

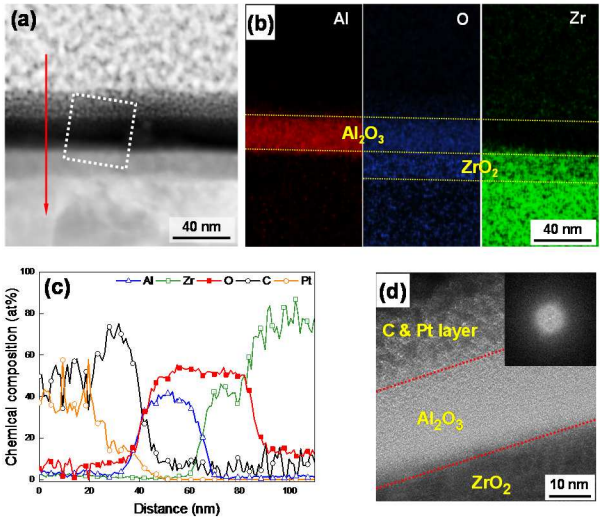

Fig. 2 TEM-EDS analysis of the Al_2O_3-coated cladding: (a) dark field TEM image, (b) elemental mapping images, (c) EDS line profiles (red arrow) and (d) TEM micrograph (white dotted box). The inset in Fig. 2(d) is a FFT image on the Al_2O_3 layer.

The surface zeta potentials and contact angles of the uncoated and Al_2O_3-coated specimens were compared in Table 1. Both surfaces were all negatively charged under the same test condition. The surface zeta potential was approximately -43.5 mV for the uncoated specimen and -52.1 mV for the Al_2O_3-coated one. The zeta potential of the magnetite particles was measured to be about -36.0 mV. The difference in the zeta potential between magnetite particle and cladding surface was larger on the coated surface than the uncoated one. This means that the Al_2O_3-coated surface has larger repulsive force with magnetite particle than the uncoated surface. The contact angle of the uncoated surface was measured with 72±1°, while the Al_2O_3-coated surface showed a slightly higher value of 85±1°. This implies that the Al_2O_3-coated surface has a slightly more hydrophobic property.

Table 1. Surface zeta potentials and water contact angles of the uncoated and Al_2O_3-coated claddings.

	Uncoated	Al_2O_3-coated
Surface zeta potential (mV)	-43.5 ± 1.1	-52 ± 1.6
Contact angle (deg.)	72 ± 1	85 ± 1

Fig. 3 shows the surface SEM images of the deposits on the uncoated and Al_2O_3-coated specimens after the deposition tests. Polyhedral particles with various sizes were uniformly deposited on both specimens, but the uncoated specimen showed higher density of the particles than the Al_2O_3-coated one. Boiling chimneys were observed more frequently on the uncoated specimen than the Al_2O_3-coated one. Furthermore, much smaller particles were observed to be deposited around the boiling chimneys. These deposits were analyzed to be mainly magnetite by XRD patterns, as shown in Fig. 4. The relatively less intensive peaks of magnetite were recorded on the Al_2O_3-coated specimen, indicating that the amount of the deposits decreased by the Al_2O_3 coating. The zirconium and its oxide (ZrO_2) peaks were also observed, which can be originated from the matrix and internally grown oxide during the deposition test, respectively. The peak intensity of ZrO_2 was relatively weak on the Al_2O_3-coated specimen compared to the uncoated one.

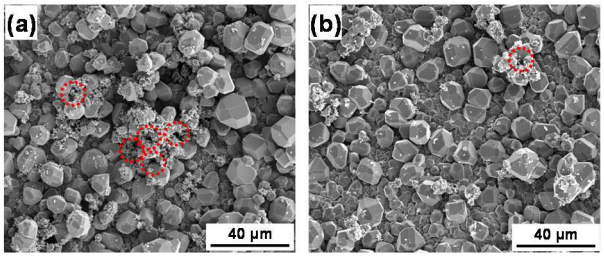

Fig. 3 SEM micrographs of the deposits on the cladding specimens after the deposition tests: (a) uncoated cladding, and (b) Al_2O_3-coated cladding. Red dotted circles indicate the boiling chimneys.

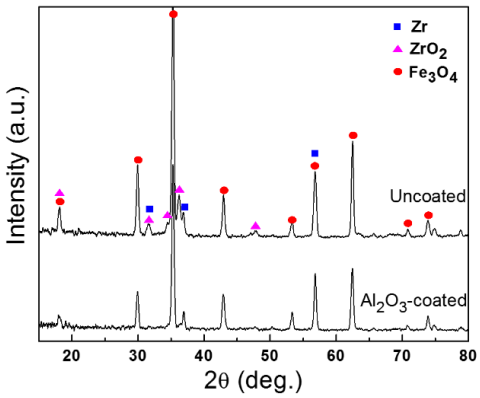

Fig. 4. XRD patterns of the uncoated and Al_2O_3-coated claddings after the deposition tests.

These results are well supported by the quantity of deposits on both the uncoated and Al_2O_3-coated specimens after the deposition tests as summarized in Table 2. The amount of deposits decreased by about 23 % for the Al_2O_3-coated specimen, comparing to the uncoated specimen. This result means that crud deposition is dependent on the surface property of the cladding. Moreover, the thickness of ZrO_2 layer on Al_2O_3-coated specimen was thinner by about 12% than that on the uncoated one after deposition test for 168 h (Table 2). At this time, the ZrO_2 thickness was measured by TEM analysis for the cross-sections of both the uncoated and Al_2O_3-coated specimens.

Table 2. Deposit mass and ZrO_2 thickness of the uncoated and Al_2O_3-coated claddings after crud deposition tests for 168 h.

	Uncoated	Al_2O_3-coated
Amount of deposit (mg/cm^2)	1.89 ± 0.06	1.45 ± 0.05
ZrO_2 thickness (nm)	652 ± 23	580 ± 20

Fig. 5 shows the cross sectional TEM image of the deposits on the Al_2O_3-coated specimen, which were vertically milled using FIB. EDS line profile was done to obtain chemical compositions along a-b. The profiles indicate that the upper bright part is magnetite and the lower dark part is zirconium oxide. It is striking that the Al_2O_3 layer was not detected between Fe_3O_4 and ZrO_2.

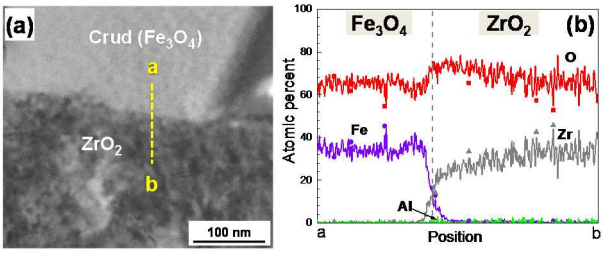

Fig. 5 TEM image on the cross section of the Al_2O_3-coated cladding and EDS profile obtained along the line a-b.

The main findings in this work can be summarized as follows: the quantity of deposits was decreased by 23% through Al_2O_3 coating but the Al_2O_3 layer disappeared after the deposition tests. The role of the Al_2O_3 coating on mitigation of crud deposition can be discussed from the viewpoint of surface properties such as zeta potential and wettability.

The surface zeta potential, which indicates electro-static force of magnetite particle toward a material surface, is an important influence factor for crud deposition on fuel claddings. The difference of zeta potentials between magnetite particle and cladding surface increased from 7.5 mV to 16.1 mV when the Al_2O_3 thin layer was coated on cladding surface. This means that the repulsive force between magnetite and cladding surface increases by Al_2O_3 coating. Therefore, transportation and adhesion of magnetite particles onto the Al_2O_3-coated surface is disfavored, resulting in a decrease in crud deposition. Although the zeta potentials were measured at 25°C, it will be effective at the higher temperature tested in this work.

The water contact angles were increased from 72° to 85° by Al_2O_3 coating as summarized in Table 1. A high contact angle corresponds to a low surface wettability. This indicates that the Al_2O_3-coated surface has a slightly more hydrophobic property. The deposit formation on a heated surface during nucleate boiling was caused from the evaporation of a micro-layer of liquid beneath a bubble, according to the micro-layer evaporation and dry-out model [18,19]. Therefore, the crud deposition amount will be strongly dependent on bubble dynamics. According to experimental observations and numerical simulations [20,21], the active nucleation site density for bubbles is proportional to the contact angle. However, the effect of contact angle on the bubble departure frequency is still controversial whether it increases or decreases with increasing the contact angle. If all the bubble density and emission frequency are enhanced on a hydrophobic surface, the crud deposition will be increased on the Al_2O_3-coated surface. However, this is not the case for our result. Therefore, it might seem that these two factors exert a competing effect. In addition, the wettability differences measured in the present work might be too small to have practical importance.

The EDS line profiles shown in Fig. 5 indicate that the coated Al_2O_3 layer was disappeared after the deposition tests. This was an unexpected result at the stage of the experiment design. The absence of Al_2O_3 layer may imply that the layer is thermodynamically unstable in this test condition and dissolves out in the test solution. Thus we checked the thermodynamic stability of Al_2O_3 in the potential-pH diagrams for the aluminum-water system at 25°C and 300°C [22]. The pH of the test solution used in this work is 6.4 at 25°C and 7.0 at 300°C, where the pH at 300°C was calculated by using MULTEQ code. Al_2O_3 is stable at pH 6.4 and 25°C, but it is no longer stable and dissolves into the AlO_2^- form at pH 7.0 and 300°C. Therefore, it can be concluded that the coated Al_2O_3 layer was gradually dissolved in the test solution during the deposition tests owing to its thermodynamic instability at elevated temperatures. When selecting coating materials, we considered only the following properties: their neutron cross section, thermal expansion coefficient, and thermal conductivity. Consequently, this result provides a painful but obvious lesson that it must be considered a thermodynamic stability of a coating material in the water chemistry condition of a PWR core in selecting step. If the coated Al_2O_3 layer were thermodynamically stable at elevated temperatures, crud deposition would be decreased even more by the Al_2O_3 coating.

On the other hand, zirconium oxide is internally grown on Zr-based cladding tubes exposed to a high temperature primary coolant. In this work, zirconium oxide layer on the Al_2O_3-coated specimen was approximately 12 % thinner than that on the uncoated one. This indicates that the coated layer delayed the oxidation of the cladding despite its thermodynamic instability.

4. Conclusions

We have investigated the role of Al_2O_3 thin layer deposited on fuel cladding on the crud deposition mitigation. The quantity of deposits on the Al_2O_3-coated claddings decreased by 23% compared with that on the uncoated cladding. The difference of zeta potentials between magnetite particle and cladding surface increased from 7.5 mV to 16.1 mV through coating the Al_2O_3 layer. Therefore, the reduction of crud deposition can be attributed to the increased repulsive force between the magnetite particle and Al_2O_3-coated cladding surface. The static contact angle on the cladding surfaces was increased from 72° to 85° by Al_2O_3 coating. However, the Al_2O_3-coated layer was dissolved into the test solution due to its thermodynamic instability at higher temperature. Nevertheless, the coated layer retarded the oxidation rate of the fuel cladding. Therefore, the simulation tests for crud deposition performed in this work show that appropriate coatings will provide a promising future for mitigation of both crud deposition and cladding oxidation in the primary solution.

Acknowledgments

This work was supported by the National Research Foundation of Korea (NRF) grant funded by the Korea government (2017M2A8A4015159).

REFERENCES

[1] S. Odar, Crud in PWR/VVER coolant, Vol. 1, Technical Report, ANT Int'l, Sweden, 2014.
[2] J. Deshon, Evaluation of Fuel Clad Corrosion Product Deposits and Circulating Corrosion Products in Pressurized Water Reactors, TR-1009951, EPRI, Palo Alto, 2004.
[3] J. Deshon, PWR Axial Offset Anomaly (AOA) Guidelines, Rev. 1, TR-1008102, EPRI, Palo Alto, CA, 2004.
[4] J. A. Sawicki, Evidence of Ni2FeBO5 and m-ZrO2 precipitates in fuel rod deposits in AOA-affected high boiling duty PWR core, J. Nucl. Mater. Vol. 374, pp. 248, 2008.

[5] Z. Rák, E. W. Bucholz, D. W. Brenner, Defect formation in aqueous environment: Theoretical assessment of boron incorporation in nickel ferrite under conditions of an operating pressurized water nuclear reactor (PWR), J. Nucl. Mater. Vol. 461, pp. 350, 2015.
[6] T. R. Allen, R. J. Konings, A. T. Motta, Corrosion of Zirconium Alloys, Comprehensive Nucl. Mater. Vol. 5, pp. 49, 2012.
[7] K. Edsinger, C. R. Stanek, B. D. Wirth, Light water reactor fuel performance: current status, challenges, and future high fidelity modelling, J. Miner, Met. Mater. So. Vol. 63, pp. 49, 2011.
[8] J. Sevens, D. Farnsworth, J. Bosma, J. Deshon, Elevated RCS pH program at Comanche Peak, Proc. Int. Conf. on Water Chemistry of Nuclear Reactor Systems, JeJu, Korea, 2006.
[9] EPRI, Pressurized Water Reactor Primary Water Chemistry Guidelines, Vol. 1, Rev. 7, TR-3002000505, Palo Alto, CA, USA, 2014.
[10] J. Deshon, K. Edsinger, P. Frattini, D. Hussey and C. J. Wood, Ultrasonic fuel cleaning in PWRs and BWRs, Proc. Int. Conf. on Water Chemistry of Nuclear Reactor Systems, Jeju, Korea, 2006.
[11] A. Uehira, M. Kanzaki, K. Kitamura, H. Anada, Pre-Filming Method of Reducing Metal Release from Alloy 690 for SG in Primary Water of PWR, ISOE North American ALARA Symposium, Fort Lauderdale, FL, 2009.
[12] C. J. Wood, Electropolishing Process Development for PWR Steam Generator Channel Heads, EPRI, NP-6619, Palo Alto, CA, 1991.
[13] M. J. Seo, H.-S. Shim, H. M. Kim, S. I. Hong, D. H. Hur, Influence of surface roughness on the corrosion behavior of Alloy 690TT in PWR primary water, Nucl. Eng. Design Vol. 280, pp. 62, 2014.
[14] C. Tang, M. Stueber, H. J. Seifert, M. Steinbrueck, Protective coatings on zirconium-based alloys as accident-tolerant fuel (ATF) claddings, Corros. Rev. Vol. 35, pp. 141, 2017.
[15] I. Dumnernchanvanit, N. Q. Zhang, S. Robertson, A. Delmore, M. B. Carlson, D. Hussey, M. P. Short, Initial experimental evaluation of crud-resistant materials for light water reactors, J. Nucl. Mater. Vol. 498, pp. 1, 2018.
[16] S. H. Baek, K. Wu, H.-S. Shim, D. H. Lee, J. G. Kim, D. H. Hur, Acoustic emission monitoring of water boiling on fuel cladding surface at 1 bar and 130 bar, Measurement, Vol. 109, pp. 18, 2017.
[17] M. S. Park, H.-S. Shim, S. H. Baek, J. G. Kim, D. H. Hur, Effects of oxidation states of fuel cladding surface on crud deposition in simulated primary water of PWRs, Ann. Nucl. Energy Vol. 103, pp. 275, 2017.
[18] Y. Asakura, M. Kikuchi, S. Uchida, H. Yusa, Deposition of iron oxide on heated surfaces in boiling water, Nucl. Sci. Eng. Vol. 76, pp. 1, 1978.
[19] S. Uchida, Y. Asakura, H. Suzuki, Deposition of boron on fuel rod surface under sub-cooled boiling conditions – an approach toward understanding AOA occurrence, Nucl. Eng. Des. Vol. 241, pp. 2398, 2011.
[20] A. R. Betz, J. Jenkins, C. J. Kim, D. Attinger, Boiling heat transfer on superhydrophilic, superhydrophobic and superbiphilic surfaces, Int. J. Heat Mass Transfer Vol. 57, pp. 733.
[21] C. H. Wang, V. K. Dhir, Effect of surface wettability on active nucleation site density during pool boiling of water on a vertical surface, J. Heat Transfer Vol. 115, pp. 659.
[22] D. Macdonal, P. Burlar, The thermodynamics of the aluminum-water system at elevated temperatures, Corrs. Sci. Vol. 13, pp. 259, 1973.